

PROCEEDINGS OF THE  
15<sup>th</sup> INTERNATIONAL  
CONFERENCE  
ON NUCLEAR REACTION  
MECHANISMS

Varenna (Italy), Villa Monastero  
June 11–15, 2018

*Edited by*  
F. Cerutti, A. Ferrari, T. Kawano, F. Salvat-Pujol, and P. Talou



CERN  
Geneva  
2019

# Transfer reactions induced with $^{56}\text{Ni}$ : shell gaps and np pairing

A. Georgiadou<sup>1</sup>, M. Assié<sup>1</sup>, Y. Blumenfeld<sup>1</sup>, B. Le Crom<sup>1</sup>, J. Guillot<sup>1</sup>, F. Flavigny<sup>1</sup>, L. Achouri<sup>2</sup>, M. Aouadi<sup>2</sup>, B. Bastin<sup>3</sup>, A. Benitez<sup>4</sup>, R. Borcea<sup>5</sup>, W. Catford<sup>6</sup>, E. Clement<sup>3</sup>, A. Corsi<sup>7</sup>, G. Defrance<sup>3</sup>, M-C. Delattre<sup>1</sup>, F. Delaunay<sup>2</sup>, N. De Séréville<sup>1</sup>, Q. Deshayes<sup>2</sup>, B. Fernandez<sup>8</sup>, M. Fisichella<sup>9</sup>, S. Franchoo<sup>1</sup>, J. Gibelin<sup>2</sup>, A. Gillibert<sup>7</sup>, F. Hammache<sup>1</sup>, O. Kamalou<sup>3</sup>, A. Knapton<sup>6</sup>, V. Lapoux<sup>7</sup>, S. Leblond<sup>2</sup>, M. Marques<sup>2</sup>, A. Matta<sup>6</sup>, P. Morfouace<sup>1</sup>, N. Orr<sup>2</sup>, J. Pancin<sup>3</sup>, X. Pereira<sup>2,8</sup>, L. Perrot<sup>1</sup>, E. Pollacco<sup>6</sup>, D. Ramos<sup>7</sup>, T. Roger<sup>3</sup>, F. Rotaru<sup>5</sup>, J-A. Scarpaci<sup>10</sup>, M. S  noville<sup>7</sup>, O. Sorlin<sup>3</sup>, M. Stanoiu<sup>5</sup>, I. Stefan<sup>1</sup>, D. Suzuki<sup>1</sup>, J-C. Thomas<sup>3</sup>, M. Vandebr  uck<sup>3</sup>, G. Verde<sup>1</sup>

<sup>1</sup>Institut de Physique Nucl  aire d'Orsay, Universit   Paris-Sud-CNRS/IN2P3, 91406 Orsay, France

<sup>2</sup>Laboratoire de Physique Corpusculaire de Caen, ENSICAEN-CNRS/IN2P3, 14050 Caen, France

<sup>3</sup>Grand Acc  l  rateur National d'Ions Lourds, CEA/DSM-CNRS/IN2P3, 14076 Caen, France

<sup>4</sup>Centro de F  sica Nuclear da Universidade de Lisboa, 1649-003 Lisboa, Portugal

<sup>5</sup>Horia Hulubei National Institute of Physics and Nuclear Engineering, Magurele, Romania

<sup>6</sup>Department of Physics, University of Surrey, Guildford GU2 5XH, United Kingdom

<sup>7</sup>Service de Physique Nucl  aire, CEA-Saclay/IRFU, 91191 Gif-sur-Yvette, France

<sup>8</sup>Universidade de Santiago de Compostela, E-15782 Santiago de Compostela, Spain

<sup>9</sup>Laboratori Nazionali del Sud, Istituto Nazionale di Fisica Nucleare, Catania, Italy

<sup>10</sup>Centre de Sciences Nucl  aires et Sciences de la Mati  re, Universit   Paris-Sud-CNRS/IN2P3, 91406 Orsay, France

## Abstract

The structure of the unstable doubly magic nucleus  $^{56}\text{Ni}$  has been investigated by measuring one- and two-nucleon transfer reactions. The radioactive beam of  $^{56}\text{Ni}$  was produced at GANIL-Caen, France at 30 MeV/u by means of the LISE spectrometer. The experimental set-up used consists of the TIARA-MUST2-EXOGAM combination which provides an almost  $4\pi$  coverage and the ability to perform particle- $\gamma$  coincidences. To probe the  $N=28$  gap, we studied the spectroscopy of  $^{55}\text{Ni}$  through one-nucleon transfer reactions on  $^{56}\text{Ni}$ . The excitation energy spectrum is deduced by measuring the light ejectiles only, while particle- $\gamma$  coincidences are used to improve the resolution of the populated states and select the main ones. Comparison between the extracted angular distributions and DWBA calculations allows the extraction of the spectroscopic strength of the hole- and particle- states populated by these one neutron pick-up reactions.

## 1 Introduction

Historically, nuclear reactions were performed, by using light ion beams on the target consisting of the nuclei of interest. As to be able to study short-lived nuclei far from stability one has to inverse the problem. That led to the use of the inverse kinematics where the target consist of the light ion and the beam is produced by the short-lived unstable nuclei or else the radioactive exotic beam.

The last three decades inverse kinematics have been used to reveal the properties of the radioactive nuclei in exotic regions of the nuclear chart, such as the drip-lines, and initialized the ability to study the shell evolution far from stability [1].

In this work with the use of one- and two-nucleon transfer reactions we study two different physical aspects. The doubly magic nucleus  $^{56}\text{Ni}$ , with  $N = Z = 28$  [2,3], makes an excellent probe for studying the  $N = 28$  shell closure next to stability as well as the neutron-proton (np) pairing correlations.

The Ni isotopic chain provides a variety of doubly magic nuclei. From the proton drip-line and  $^{48}\text{Ni}$  lying in the edge of the particle-stability and being the mirror nucleus of  $^{48}\text{Ca}$ , to the  $N = Z$   $^{56}\text{Ni}$

and finally  $^{78}\text{Ni}$  lying in the neutron-drip line. The shell evolution of the  $N = Z = 28$  has been of great interest the recent years. With new experimental results on the neutron drip line, the  $Z = 28$  magic shell reveals a resistive strength making  $^{78}\text{Ni}$  the most neutron rich doubly magic nucleus [4]. Although as one moves to the edges of the nuclear chart the  $N = 28$  shell closure becomes questionable and a quenching of the single-particle states is expected to take place.

One-nucleon transfer reactions such as (d,p), (p,d) and (d,t) are one of the most direct ways to test the single particle configuration of the magic nucleus  $^{56}\text{Ni}$ . Measuring the occupancy and vacancy of neutron orbits will provide information on the robustness of the  $N = 28$  magic number through the  $N=27$  and  $N=29$  isotones.

The structural evolution studied with  $N=27$  isotones for  $^{48}\text{Ca}$  is described in detail in the review paper of O.Sorlin and M-G. Porquet [5]. It is noted specifically that about 90% of the ground state configuration of the spherical  $^{47}\text{Ca}$  nucleus corresponds to a neutron hole inside the  $f_{7/2}$  shell (0p1h configuration) and a closed proton core (0p0h configuration). They presented a possible development of collectivity in the  $N = 27$  isotones, by comparing the characteristics of their first states.

The first excited state with  $J^\pi = 3/2^-$  is expected to involve the promotion of one neutron in the upper  $p_{3/2}$  shell with two neutron holes coupled in the  $f_{7/2}$  shell (1p2h). This agrees with theoretical calculation showing that the strength lies mainly in the pure excitation of one neutron and less from three neutrons [6, 7]. This state, with closed proton configuration, would be found well above the ground state of all the  $N=27$  isotones, except if the  $N=28$  shell gap is reduced and there is domination by the correlations. As it is shown in the same study it is the case for the  $N=27$  isotones in the  $sd$  shell.

Experimentally, the measurement of the cross sections for one-nucleon transfer have to be compared with theoretical calculations to compare the experimental ones. The ratio in between the two values give the Spectroscopic factor of the single particle state of interest that can later be used to reveal the neutron occupancy.

## 2 Experimental Case

The experiment was performed in 2014 in Grand Accélérateur National d'Ions Lourds (GANIL), Caen. The radioactive beam of  $^{56}\text{Ni}$  at 30 MeV/u was produced by fragmentation of a primary beam of  $^{58}\text{Ni}$  and purified by means of the LISE3 separator [8]. Measurements were performed in inverse kinematics on  $\text{CH}_2$  and  $\text{CD}_2$  targets. Two beam tracking multiwire proportional chambers (CATS) were placed upstream of the reaction target and yielded event by event the position and angle of the incoming beam particles [9].

The experiment included close to  $4\pi$  coverage for the light charged ejectiles. The two components of the double sided silicon strip detector (DSSSD) TIARA, Barrel and Hyball, were placed at central and backward angles [10], while four telescopes of the DSSSD MUST2 covered the forward angles [11]. Tiara and MUST2 provided the necessary parameters for extracting excitation energy and angular distribution.

Around the target 4 germanium clovers of EXOGAM were used for particle- $\gamma$  coincidences in order to identify the populated state of the residue and disentangle the excited states [12]. At the end of the beam line the Si-Si-CsI telescope CHARISSA was placed to detect heavy residues (although it was not used in the current analysis). The energy loss, residual energy, angle and time of flight were measured in order to perform particle identification.

## 3 One-nucleon transfer reactions

### 3.1 Reaction Kinematics

The kinematic lines are unique for any two-body reaction. They give the identification of light ejectiles which consequently add to the identification of the populated levels of the residue nucleus. Hereby,

we present the kinematics obtained for the one nucleon transfer reactions (d,t) and (p,d) at 30 MeV per nucleon on a 7 mg/cm<sup>2</sup> CD<sub>2</sub> and 6.8 mg/cm<sup>2</sup> CH<sub>2</sub> target respectively (see Figure 1). The experimental kinematic lines of the one nucleon transfer reactions show the population of the ground state, as well as the first excited states and also allow us to compare the two different reactions populating the same nucleus <sup>55</sup>Ni. In the experimental spectra, with red and green we identify the ground state and one of the excited states, the 3.185 MeV, respectively.

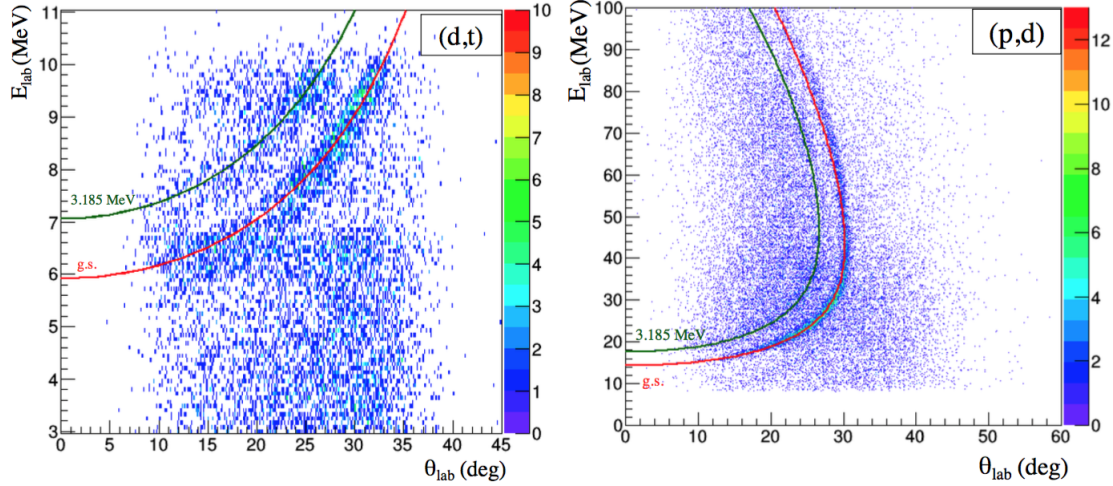


**Fig. 1:** Kinematic lines of one-nucleon transfer reactions. Left: for the (d,t). Right: of the (p,d) reactions. Red line is the theoretical expected kinematic line for the ground state while with green the excited state of 3.185 MeV is being depicted.

### 3.2 Excitation Energy

For the (d,t) reaction the excitation energy spectrum is shown in the left of Figure 2. The separation in between the ground state and the excited states is clear with the ground state peak resolution being 1.8 MeV (FWHM) and in a relatively good agreement with the simulation if we consider the uncertainty on the beam energy resolution in the simulations. The CD<sub>2</sub> target has a thickness of 7 mg/cm<sup>2</sup>, this adds the effect of straggling of the light ejectile in the target and that is why the energy resolution is not the one expected for MUST2 detector.

For the (p,d) reaction the excitation energy spectrum from Figure 2 (right) shows the ground state separated from the excited states as well, with the energy resolution of the ground state of 910 keV (FWHM).

The resolution of the energy peaks as well as the sparse knowledge of the level scheme of <sup>55</sup>Ni do not allow a clear picture of the population of the excited states by looking only in the particle energy spectra. In this work in addition to the particle information we were able to perform particle- $\gamma$  coincidences that allow the disentanglement of the excited state which are populated by these reactions.

### 3.3 Particle- $\gamma$ coincidences

By gating on excitation energy for the energy range 1.5 MeV to 4.5 MeV, we can identify the  $\gamma$ -ray corresponding to each energy level transition that each of these reactions populates in the particle- $\gamma$  coincidence spectrum. Some of the  $\gamma$ -rays resulting from transitions between excited states of <sup>55</sup>Ni (see Figure 3) were well identified on the spectrum with a resolution of 80 keV. We identify 3 clear separated  $\gamma$ -rays, the 735, 1100 and 2100 keV that correspond to the levels of interest. The blue numbers in Figure 3

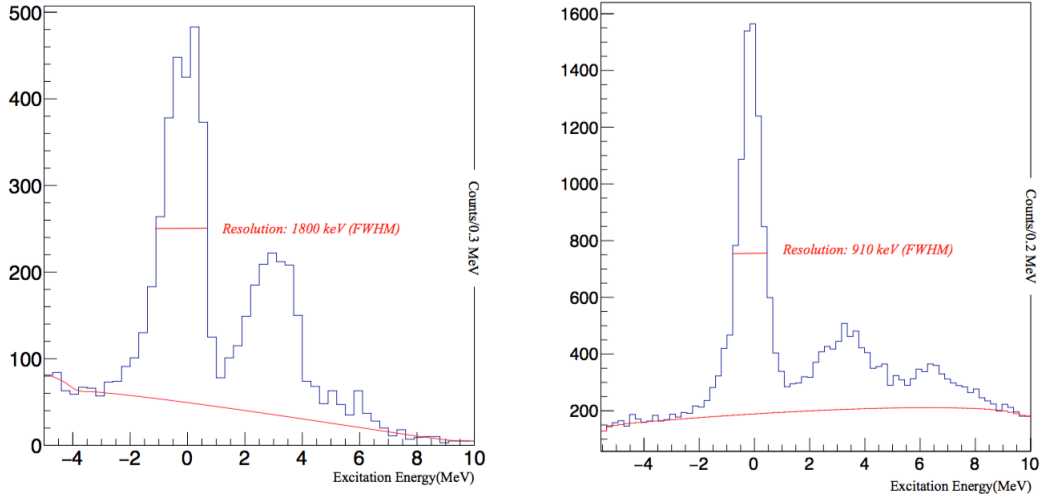


**Fig. 2:** The excitation energy plots for both one nucleon transfer. Left: Excitation energy spectrum for the (d,t) reaction. Right: Excitation energy spectrum for the (p,d) reaction. With red, the carbon background contribution is indicated and at the FWHM the resolution of each ground state.

corresponds to new measurements that we add in the level scheme of  $^{55}\text{Ni}$ . The  $\gamma$  yields are obtained by a Gaussian fit which gives the number of counts that are used to calculate the relative population for each level.

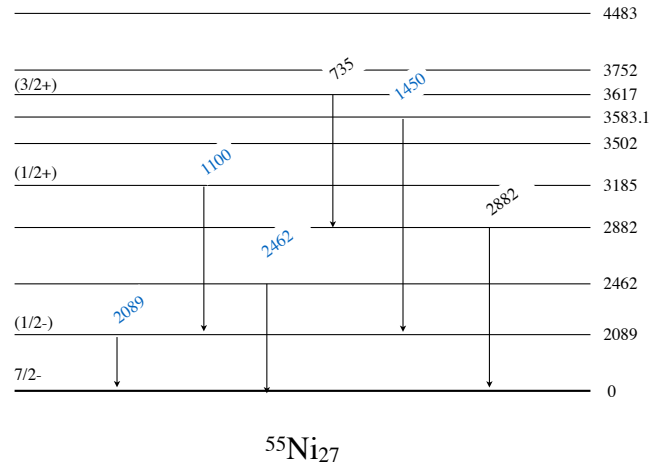


**Fig. 3:** Levels and  $\gamma$ -rays observed in this experiment. The new ones are indicated with blue and the ones already known with black (Based on ENSDF).

For the fit of each state in both reactions, we use the additional information given from the particle- $\gamma$  coincidences to identify each excited state. In the case of the (p,d) reaction, we use the information provided by the relative population of the  $\gamma$ -rays to adjust the limits of the maximum and minimum expected yields for each excited state in the particle spectra due to better statistics and larger angular coverage of this reaction channel.

### 3.4 Angular Distributions

We measure the differential cross section for  $N_{56Ni}$  incoming beam particles hitting a target with  $N_{target}$  protons or deuterons per  $cm^2$  in different angular ranges.

The angular distributions for the (d,t) and (p,d) reactions are shown in Figure 4. The measured angular distributions were compared with Distorted Wave Born Approximation calculations and the spectroscopic factors obtained can be shown in Table 1.

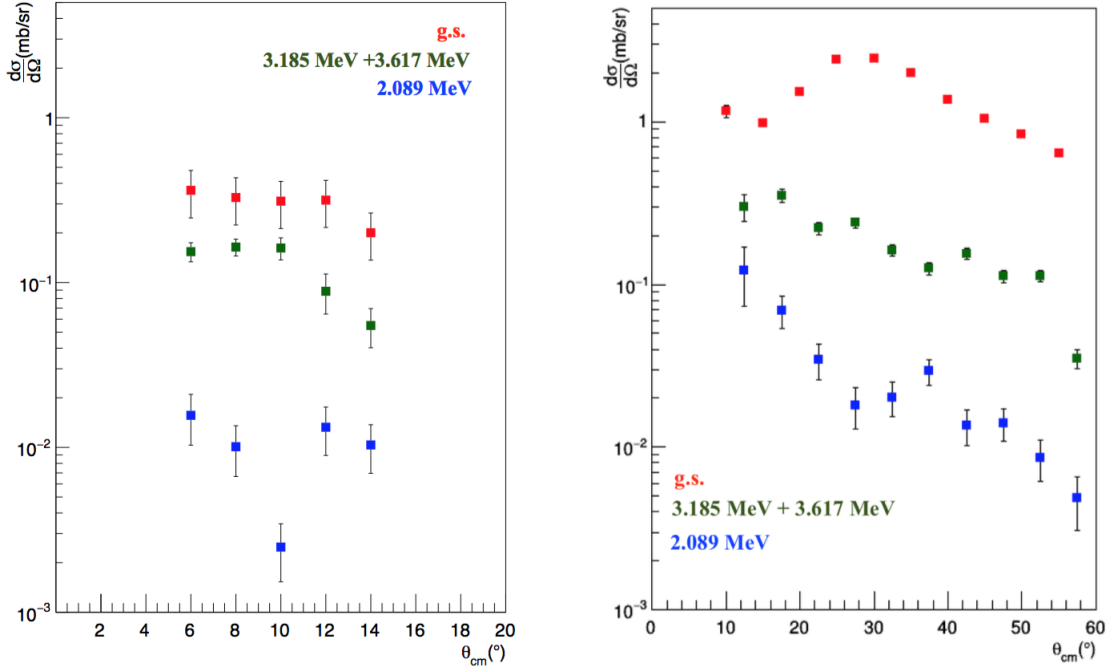


**Fig. 4:** Angular distributions for the one nucleon transfer reactions, for the ground state  $f_{7/2}$ , 2.09  $2p_{3/2}$ , 3.185  $2s_{1/2}$  together with the 3.6  $d_{3/2}$

State	$E_{exp}$ (MeV)	E (MeV) [13]	$E_{SM1}^*$ (MeV)	$SF_{exp}^{(p,d)}$	$SF_{exp}^{(d,t)}$	SF [13]	$SF_{SM1}$
$1f_{7/2}$	0.0	0.0	0.0	$5.4 \pm 1.0$	$5.8 \pm 1.2$	$6.7 \pm 0.7$	6.75
$2p_{3/2}$	2.1	2.09	1.89	$0.10 \pm 0.02$	$0.020 \pm 0.004$	$0.19 \pm 0.03$	0.13
$2s_{1/2}$	3.2	3.18	3.039	$2.0 \pm 0.4$	$0.20 \pm 0.04$	$1.0 \pm 0.2$	1.57
$1d_{3/2}$	3.617	(3.752)	3.309	$1.8 \pm 0.4$	$1.07 \pm 0.21$	-	2.88

**Table 1:** Experimental and calculated information on the  $f_{7/2}$ ,  $2p_{3/2}$ ,  $2s_{1/2}$  and  $d_{3/2}$  states. Where  $E_{exp}$ (MeV) and  $SF_{exp}$  indicated the results of this work.

The results obtained by this work for the ground state and the 2.089 MeV state, were compared with the ones obtained by A. Sanetullaev *et al.* [13]. In addition, new information about the single particle states below the N=20 gap were obtained that will allow us to study the evolution of the N=28 shell gap [14].

## 4 Conclusions

With the one-nucleon transfer reaction we obtained the spectroscopic factors for the ground state and the three excited states corresponding to the removal of a neutron in the  $1f_{7/2}$ ,  $2p_{3/2}$ ,  $2s_{1/2}$  and  $1d_{3/2}$  via the

(d,t) and (p,d) reactions. The combined information from particle- $\gamma$  coincidences, allowed us to enrich the level scheme of  $^{55}\text{Ni}$  and disentangle the different energy levels. We are able now to investigate the evolution of the N=28 shell gap by comparing spectroscopic factors obtained by previous measurements all along the  $fp$  shell for the N=27 isotones with Z=20 until Z=28.

## 5 Perspectives

$^{56}\text{Ni}$ , as an N=Z nucleus with fully closed shell, is a key nucleus to investigate neutron-proton pairing in the largest shell accessible experimentally, the  $fp$  shell. Neutron-proton pairing can occur both in the isoscalar (T=0) and in the isovector (T=1) channels. The relative intensity of both channels reveals the collective nature of the states. However angular distribution for the state  $J=0^+, T=1$  and  $J=1^+, T=0$  states are highly desirable to disentangle the reaction mechanism [15]. We have previously measured the two-nucleon transfer reaction  $^{56}\text{Ni}(p, ^3\text{He})^{54}\text{Co}$  [16] and anew analysed the  $^{56}\text{Ni}(d, \alpha)^{54}\text{Co}$ . In the (p, $^3\text{He}$ ) reaction, the ratio of the population of the T=0 and T=1 states indicates a predominance of T=1 isovector pairing weakening of the strength in the T=0 channel. The selectivity in  $\Delta T=0$  of the (d, $\alpha$ ) reaction enables further investigation of the isoscalar channel contribution. The results for the transfer reaction  $^{56}\text{Ni}(d, \alpha)^{54}\text{Co}$  will complete the information about the strength of the isoscalar neutron-proton pairing and will be expected to show that the cross-sections are low in the  $fp$  shell.

## References

- [1] A. Obertelli, *Eur. Phys. J. Plus* (2016) 131: 319
- [2] M. Mayer, *Phys. Rev.*, 74:235-239 (1948)
- [3] M. Mayer, *Phys. Rev.*, 75:1969-1970 (1949)
- [4] L. Olivier *et al.*, *Phys. Rev. Lett.* 119, 192501
- [5] O. Sorlin and M. -G. Porquet, *Phys. Scripta*, Vol. T152 (2013)
- [6] F. Nowacki and A. Poves, *Phys. Rev. C*, 79 014310 (2009)
- [7] L. Gaudefroy *et al.*, *Phys. Rev. C*, 78 034307(2008)
- [8] R. Anne *et al.*, *NIM A*, 257(2):2150-232, (1987)
- [9] S. Ottini-Hustache *et al.* *NIM A*, 431:476-484, (1999)
- [10] M. Labiche *et al.*, *NIM B*, 614:439-448, (2010)
- [11] E. Pollacco *et al.*, *Eur. Phys. J.*, 25(10.1140/epjad/i2005-06-162-5):287-288, (2005).
- [12] F. Azaiez, *Nuclear Physics A*, 654 (1999) 1003c-1008c
- [13] A. Sanetullaev *et al.*, *Physics Letters B* 736 (2014) 137-141
- [14] A. Georgiadou, PhD thesis, Université Paris-Saclay, Institut de Physique Nucléaire, CNRS/IN2P3/Université Paris-Sud XI, 91406 Orsay Cedex, (2018)
- [15] G. Potel *et al.* *Reports on Progress in Physics*, 76(10):106301, (2013)
- [16] B. Le Crom, PhD thesis, Université Paris-Saclay, Institut de Physique Nucléaire, CNRS/IN2P3/Université Paris-Sud XI, 91406 Orsay Cedex, (2016)